

# Exploring neutralino dark matter resonance annihilation via $bA, bH \rightarrow b\mu^+\mu^-$ at the LHC

Howard Baer<sup>1\*</sup>, Alexander Belyaev<sup>2†</sup>, Chung Kao<sup>1‡</sup> and Patrik Svantesson<sup>2§</sup>

<sup>1</sup> *Homer L. Dodge Department of Physics and Astronomy, University of Oklahoma, Norman, OK 73019, USA*

<sup>2</sup> *NExT Institute: School of Physics & Astronomy, Univ. of Southampton, UK  
Particle Physics Department, Rutherford Appleton Laboratory, UK*

## Abstract

One of the main channels which allows for a large rate of neutralino dark matter annihilation in the early Universe is via the pseudoscalar Higgs  $A$ -resonance. In this case, the measured dark matter abundance can be obtained in the minimal supergravity (mSUGRA) model when  $\tan\beta \sim 50$  and  $2m_{\tilde{Z}_1} \sim m_A$ . We investigate the reaction  $pp \rightarrow b\phi \rightarrow b\mu^+\mu^- + X$  (where  $\phi = A$  or  $H$ ) at the CERN LHC where requiring the tag of a single  $b$ -jet allows for amplification of the signal-to-background ratio. The rare but observable Higgs decay to muon pairs allows for a precise measurement of the Higgs boson mass and decay width. We evaluate signal and background using CalcHEP, with muon energy smearing according to the CMS detector. We find that the Higgs width ( $\Gamma_A$ ) can typically be determined with the accuracy up to  $\sim 8\%$  ( $\sim 17\%$ ) for  $m_A \sim 400$  (600) GeV assuming  $10^3 \text{ fb}^{-1}$  of integrated luminosity. Therefore, the  $pp \rightarrow b\phi \rightarrow b\mu^+\mu^- + X$  process provides a unique possibility for direct  $\Gamma_A$  measurement at the LHC. While the Higgs width is correlated with the parameter  $\tan\beta$  for a given value of  $m_A$ , extracting  $\tan\beta$  is complicated by an overlap of the  $A$  and  $H$  peaks, radiative corrections to the  $b$  and  $\tau$  Yukawa couplings, and the possibility that SUSY decay modes of the Higgs may be open. In the case where a dilepton mass edge from  $\tilde{Z}_2 \rightarrow \ell^+\ell^-\tilde{Z}_1$  is visible, it should be possible to test the relation that  $2m_{\tilde{Z}_1} \sim m_A$ .

PACS numbers: 14.80.Ly, 12.60.Jv, 11.30.Pb

---

\*Email: baer@physics.ou.edu

†Email: a.belyaev@soton.ac.uk

‡Email: kao@physics.ou.edu

§Email: p.svantesson@soton.ac.uk

# 1 Introduction

The lightest neutralino  $\tilde{Z}_1$  of  $R$ -parity conserving supersymmetric (SUSY) models is often touted as an excellent WIMP candidate for cold dark matter (CDM) in the universe [1]. However, in SUSY models where the  $\tilde{Z}_1$  is mainly bino-like, the natural value of the relic density  $\Omega_{\tilde{Z}_1} h^2$  is in the 1-100 range [2], which is far beyond the WMAP observation [3],

$$\Omega_{CDM} h^2 \equiv \rho_{CDM}/\rho_c = \Omega_{CDM} h^2 = 0.1123 \pm 0.0035 \quad 68\% \text{ CL}, \quad (1)$$

where  $h = 0.74 \pm 0.03$  is the scaled Hubble constant [4]. To gain accord between theory and observation, special neutralino annihilation mechanisms must be invoked. These include: (i). co-annihilation (usually involving  $\tilde{Z}_1$  with a stau [5], stop [6] or chargino [7]), (ii). tempering the neutralino composition [8] so it is a mixed bino-higgsino (as occurs in the hyperbolic branch/focus point (HB/FP) region of mSUGRA [9]) or mixed bino-wino state or (iii). annihilation through the light ( $h$ ) or heavy Higgs boson resonance ( $A$  and/or  $H$ ) [10].

In this paper, we are concerned with testing the latter annihilation mechanism, which occurs if  $2m_{\tilde{Z}_1} \simeq m_A$ . The  $A$ -resonance annihilation mechanism already occurs in the paradigm minimal supergravity (mSUGRA or CMSSM) model, which serves as a template for many investigations into SUSY phenomenology. The mSUGRA parameters at the grand unification (GUT) scale include

$$m_0, m_{1/2}, A_0, \tan\beta \text{ and } \text{sign}(\mu), \quad (2)$$

where  $m_0$  is a common scalar mass,  $m_{1/2}$  is a common gaugino mass,  $A_0$  is a common trilinear term and  $\tan\beta$  is the ratio of Higgs field vacuum expectation values (VEVs). The superpotential Higgs mass term  $\mu$  has its magnitude, but not sign, determined by radiative breaking of electroweak symmetry (REWSB), which is seeded by the large top quark Yukawa coupling.

In mSUGRA, as  $\tan\beta$  increases, the  $b$ - and  $\tau$ - Yukawa couplings –  $f_b$  and  $f_\tau$  – also increase, and in fact their GUT scale values may become comparable to  $f_t$  for  $\tan\beta \sim 50$ . In this case, the up and down Higgs soft masses  $m_{H_u}^2$  and  $m_{H_d}^2$  run under renormalization group evolution to nearly similar values at the weak scale. Since at the weak scale  $m_A^2 \sim m_{H_d}^2 - m_{H_u}^2$  [11], we find that as  $\tan\beta$  increases, the value of  $m_A$  decreases [12], until finally the condition  $2m_{\tilde{Z}_1} \simeq m_A$  is reached, whereupon neutralino annihilation through the  $A$ -resonance may take place. Another condition that occurs at large  $\tan\beta$  is that since the  $b$ - and  $\tau$  Yukawa couplings are growing large, the partial widths  $\Gamma(A \rightarrow b\bar{b})$  and  $\Gamma(A \rightarrow \tau\bar{\tau})$  also grow, and the  $A$  width becomes very large (typically into the tens of GeV range). In this case, a wide range of parameter space actually accommodates  $\tilde{Z}_1\tilde{Z}_1$  annihilation through  $A$ ,  $H$ , and the value of  $2m_{\tilde{Z}_1}$  may be a few partial widths off resonance since in the relic density calculation the  $\tilde{Z}_1\tilde{Z}_1$  annihilation rate times relative velocity must be thermally averaged. The question we wish to address here is: how well may one identify the cosmological scenario of *neutralino annihilation through the heavy Higgs resonance* via measurements at the CERN LHC?

Since the  $b$ -quark Yukawa coupling increases with  $\tan\beta$ , so do the Yukawa-induced Higgs production cross sections such as  $b\bar{b} \rightarrow A$ ,  $bg \rightarrow bA$  and  $gg, q\bar{q} \rightarrow b\bar{b}A$ . The presence of additional high  $p_T$   $b$ -jets in the final state for the second and third of these reactions allows one to tag the  $b$ -quark related production mechanisms, and also allows for a cut which rejects SM backgrounds – which don't involve the enhanced  $b$  Yukawa coupling – at low cost to signal.

The second of these reactions, which is tagged by a single  $b$ -jet in the final state, occurs at an order of magnitude greater cross section than  $b\bar{b}A$  production at the LHC [13].

The  $A$  and  $H$  Higgs bosons are expected to dominantly decay to  $b\bar{b}$  and  $\tau\bar{\tau}$  final states. Then, the  $b\bar{b}\bar{b}$  or  $b\tau\bar{\tau}$  modes offer a substantial LHC reach for  $A$  and  $H$ , especially at large  $\tan\beta$  [14]. Along with these decay modes, the decay  $A, H \rightarrow \mu^+\mu^-$  has been found to be very useful [15]. Since the  $f_\mu$  Yukawa coupling constant also increases with  $\tan\beta$ , this mode maintains its branching fraction – typically at the  $10^{-4}$  level – even in the face of increasing  $A \rightarrow b\bar{b}$  partial width. It also offers the advantages in that the two high  $p_T$  isolated muons are easy to tag, and the reconstruction of the invariant mass of muon pair,  $m_{\mu^+\mu^-}$ , allows a high precision measurement of the  $A$  mass and width,  $\Gamma_A$ . In fact, it was shown in Ref. [16] that the LHC discovery potential for  $A \rightarrow \mu^+\mu^-$  is greatest in the  $b\mu^+\mu^-$  mode at large  $\tan\beta$ , compared to  $\mu^+\mu^-$ , or  $b\bar{b}\mu^+\mu^-$ . We will adopt the  $pp \rightarrow bA, bH + X$  production mode along with decay to muon pairs as a key to explore neutralino annihilation via the  $A$ -resonance in this paper.

In Fig. 1, we show the leading order cross section for  $pp \rightarrow b\phi \rightarrow b\mu^+\mu^- + X$  production versus  $m_A$  at LHC with  $\sqrt{s} = 14$  TeV. We show curves for  $\phi = A$  and  $H$ , and for  $\tan\beta = 10$  and 55. Several features are worth noting.

- The cross sections for  $A$  and  $H$  production are nearly identical, except at very low  $m_A$  values, where substantial mixing between  $h$  and  $H$  occurs.
- The total production cross section increases by a factor of  $\sim 40$  in moving from  $\tan\beta = 10$  to  $\tan\beta = 55$ . This reflects the corresponding increase in  $b$ -quark Yukawa coupling  $f_b$ , and goes as  $f_b^2$  in the total production cross section.
- In spite of the small  $A, H \rightarrow \mu^+\mu^-$  branching fraction of  $\sim 10^{-4}$ , the cross section for  $b\mu^+\mu^-$  production via the Higgs remains large, varying between over  $10^2$  fb for low  $m_A$  to  $\sim 10^{-1}$  fb for  $m_A \sim 1$  TeV when  $\tan\beta$  is large. For LHC integrated luminosities ( $L$ ) of order  $10^2 - 10^3$  fb $^{-1}$ , these rates should be sufficient at least to extract the  $A$  and/or  $H$  mass bump.
- In addition, the factorization scale and the renormalization scale are chosen to be  $\mu_F = \mu_R = m_\phi/4$  with  $\phi = A, H$ . This choice of scale effectively reproduces the effects of next-to-leading order (NLO) corrections [13].

The remainder of this paper is organized as follows. In Sec. 2, we review neutralino annihilation via the  $A$ -resonance in the mSUGRA model, and the reach of LHC for  $A, H \rightarrow \mu^+\mu^-$  in mSUGRA parameter space for various values of integrated luminosities. In Sec. 3, we present our methods and results from Monte Carlo simulations for  $A, H$  production and decay to muons. In Section 4, we present our strategy to extract Higgs masses ( $m_{A,H}$ ) and Higgs widths ( $\Gamma_{A,H}$ ), and show the expected precision that LHC might be expected to attain in measuring  $m_A$  and  $\Gamma_A$ . In Sec. 5 (Conclusions), we comment on how these measurements will help ascertain when  $A$ -resonance annihilation might be the major annihilation reaction for neutralino dark matter in the early universe.

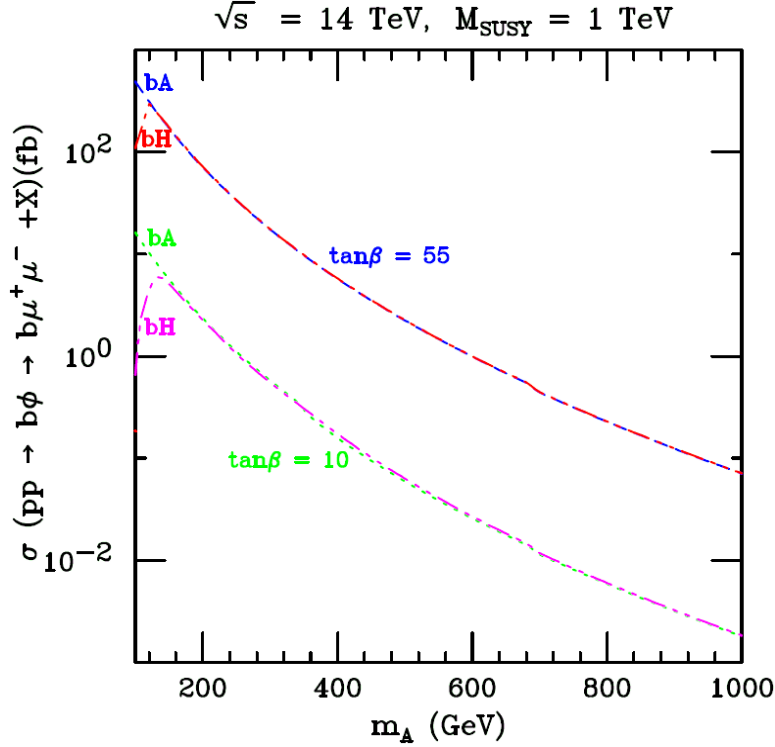


Figure 1: The total production cross section for  $pp \rightarrow b\phi \rightarrow b\mu^+\mu^- + X$  versus  $m_A$  in fb at LHC with  $\sqrt{s} = 14$  TeV. We show results for  $\phi = A$  and  $H$ , and for  $\tan\beta = 10$  and  $55$ .

## 2 The $A$ -resonance annihilation region in mSUGRA

In this section, we would like to map out the portions of the  $A$ -resonance annihilation parameter space which are potentially accessible to LHC searches. Figure 2 shows our results in the  $(m_0, m_{1/2})$  plane of the mSUGRA model for  $A_0 = 0$ ,  $\tan\beta = 55$  and  $\mu > 0$ . The green-shaded region has a relic density<sup>1</sup> of  $0.1 < \Omega_{\tilde{Z}_1} h^2 < 0.12$ , while the yellow-shaded region has  $\Omega_{\tilde{Z}_1} h^2 < 0.1$ . The red-shaded region has too large a thermal neutralino abundance  $\Omega_{\tilde{Z}_1} h^2 > 0.12$ , and so is excluded under the assumption of a standard cosmology with neutralino dark matter. The gray region is excluded because either REWSB breaks down (right side), or we find a stau as the lightest SUSY particle (LSP) (left side). The blue shaded region is excluded by LEP2 searches for chargino pair production, *i.e.*  $m_{\tilde{W}_1} < 103.5$  GeV.

The  $A$ -resonance annihilation region is plainly visible on the plot. We also show the SUSY reach of the CERN LHC assuming  $\sqrt{s} = 14$  TeV and  $100 \text{ fb}^{-1}$  of integrated luminosity, taken from Fig. 5 of Ref. [19]. The LHC reach is mainly determined by the total cross section for  $\tilde{g}\tilde{g}$ ,  $\tilde{q}\tilde{q}$  and  $\tilde{q}\tilde{q}$  production, followed by their subsequent cascade decays [20] into final states with multi-jets plus multi-isolated leptons plus missing transverse energy (MET). A hypercube of cuts is examined to extract signal and background rates over a variety of cascade decay signal channels. We see that with  $L = 100 \text{ fb}^{-1}$ , LHC can nearly cover the entire  $A$ -funnel. Doubling the integrated luminosity would allow for complete exploration of this DM-allowed region.

<sup>1</sup> The neutralino relic density is computed with the IsaReD [17] subroutine of Isajet 7.80 [18].

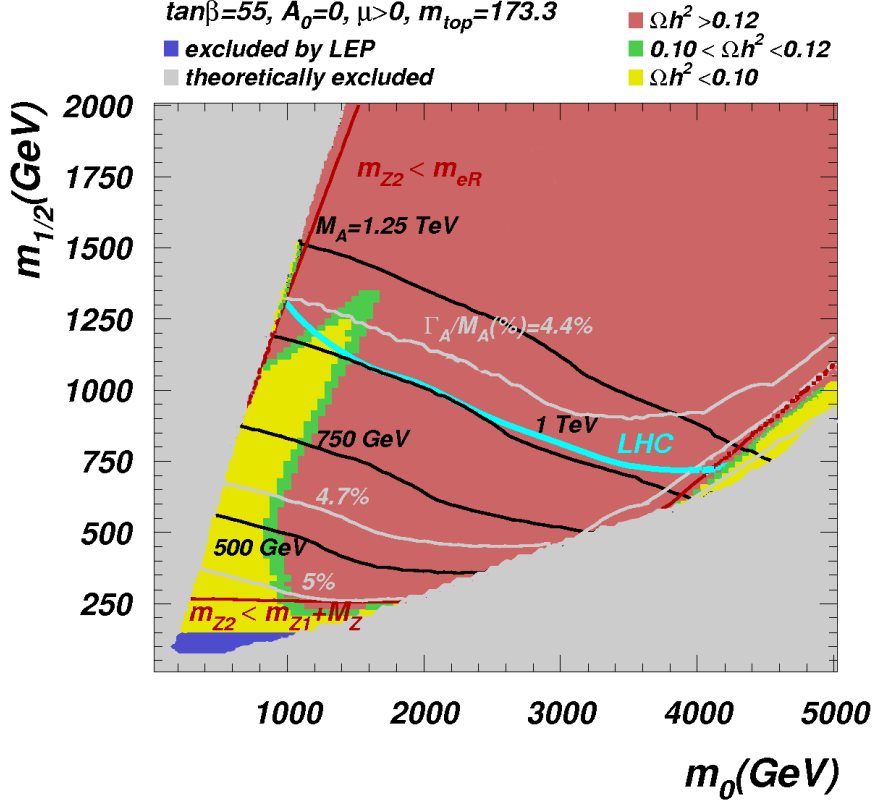


Figure 2: The  $m_0$  vs.  $m_{1/2}$  frame of the  $mSUGRA$  model for  $\tan\beta = 55$ ,  $A_0 = 0$ ,  $\mu > 0$  and  $m_t = 173.3$  GeV. The green and yellow regions provide a thermal neutralino abundance in accord with WMAP measurements of the dark matter density. We also show contours of  $m_A$  and  $\Gamma_A/m_A$ , and also show the LHC reach for SUSY with  $100 \text{ fb}^{-1}$  and  $\sqrt{s} = 14$  TeV.

Meanwhile, much of the HB/FP region is inaccessible to LHC searches, although it should be completely covered by future WIMP searches by Xe-100 and Xe-1-ton experiments [21, 22].

We also show the contour where  $m_{\tilde{Z}_2} > m_{\tilde{e}_R}$  and where  $m_{\tilde{Z}_2} < m_{\tilde{Z}_1} + M_Z$ . In the former region, the decay  $\tilde{Z}_2 \rightarrow e\tilde{e}_R \rightarrow e^+e^-\tilde{Z}_1$  will be kinematically open while in the latter region the 3-body decay  $\tilde{Z}_2 \rightarrow \tilde{Z}_1 e^+e^-$  should be visible. In either case, the dilepton mass edge  $m_{\ell^+\ell^-}$  should provide information on  $m_{\tilde{Z}_2}$  and  $m_{\tilde{Z}_1}$  [23].

Next, we would like to know how much of the  $A$ -funnel region is open to heavy Higgs detection in the  $A \rightarrow \mu^+\mu^-$  mode. A parton level study has been performed in Ref. [16] for  $m_A$  values up to 600 GeV. Here, we wish to extend these results to much higher  $m_A$  values. In Ref. [16], the maximal reach for the  $A$ ,  $H \rightarrow \mu^+\mu^-$  mode was found to be in the  $pp \rightarrow b\phi + X$  channel, where  $\phi = A$  or  $H$ .

The study in Ref. [16] evaluated  $pp \rightarrow b\phi \rightarrow b\mu^+\mu^- + X$  production against SM backgrounds coming from  $bg \rightarrow b\mu\mu$ , from  $gg, q\bar{q} \rightarrow b\bar{b}W^+W^-$  and from  $gb \rightarrow bW^+W^-$  (followed by  $W \rightarrow \mu\nu_\mu$  decay). They required the presence of

- two isolated opposite-sign muons with  $p_T > 20$  GeV and pseudorapidity  $|\eta_\mu| < 2.5$ ,

- one tagged  $b$ -jet, with  $p_T(b - jet) > 15$  (30) GeV and  $|\eta_b| < 2.5$  and  $b$ -jet detection efficiency of  $\epsilon_b = 60$  (50)% for low (high) integrated luminosity regimes,
- $MET < 20$  GeV (40 GeV), to reduce backgrounds from  $t\bar{t}$  production for low (high) integrated luminosity regimes.

The number of signal and background events within the mass range  $m_\phi \pm \Delta M_{\mu^+\mu^-}$  was examined. Here,  $\Delta M_{\mu^+\mu^-} \equiv 1.64 [(\Gamma_\phi/2.36)^2 + \sigma_m^2]^{1/2}$ , with  $\Gamma_\phi$  equal to the total width of the Higgs boson, and  $\sigma_m$  was the muon mass resolution, taken to be 2% of  $m_\phi$ . The signal is considered to be observable if the lower limit on the signal plus background is larger than the corresponding upper limit on the background with statistical fluctuations

$$L(\sigma_s + \sigma_b) - N\sqrt{L(\sigma_s + \sigma_b)} \geq L\sigma_b + N\sqrt{L\sigma_b} \quad (3)$$

or equivalently,

$$\sigma_s \geq \frac{N}{L} \left[ N + 2\sqrt{L\sigma_b} \right]. \quad (4)$$

Here  $L$  is the integrated luminosity,  $\sigma_s$  is the cross section of the signal, and  $\sigma_b$  is the background cross section. The parameter  $N$  specifies the level or probability of discovery, which is taken to be  $N = 2.5$  for a  $5\sigma$  signal. For  $\sigma_b \gg \sigma_s$ , this requirement becomes similar to

$$N_{\text{SS}} = \frac{N_s}{\sqrt{N_b}} = \frac{L\sigma_s}{\sqrt{L\sigma_b}} \geq 5,$$

where  $N_s$  is the signal number of events,  $N_b$  is the background number of events, and  $N_{\text{SS}} =$  the statistical significance, which is commonly used in the literature.

Here, at the first stage of our analysis, we repeat this calculation, although we extend the results to much higher values of  $m_\phi$  and higher integrated luminosities. We also have evaluated additional possible backgrounds to make sure that their contributions are either important or negligible. In our analysis, we use the CTEQ6L set for PDFs [24] and the QCD scale is set equal to  $m_A/4$  for signal and  $\hat{s}$  for backgrounds. The following backgrounds have been evaluated with the respective  $K$ -factors applied to take into account Higher order corrections:

- $gg + q\bar{q} \rightarrow W^+W^-b\bar{b} \rightarrow \mu^+\mu^-\nu\bar{\nu}$  ( $K = 2$ ): this is the dominant background coming mainly from  $t\bar{t}$  production and decay,
- $bg \rightarrow W^+W^-b \rightarrow \mu^+\mu^-\nu\bar{\nu}$  ( $K = 1.3$ ): this background is typically at least one order of magnitude below the first one,
- $bg \rightarrow b\mu^+\mu^-\nu\bar{\nu}$  ( $K = 1.3$ ): this background is of the same order of magnitude as previous one,
- $b\gamma \rightarrow b\mu^+\mu^-\nu\bar{\nu}$  ( $K = 1.3$ ): this background is several times lower than the previous one and can be considered as a subdominant one, contributing to the total background at the percent level. It was evaluated using the photon distribution function of the proton available in CalcHEP,

- $cg \rightarrow c\mu^+\mu^-\nu\bar{\nu}$  ( $K = 1.3$ ): this background is of the same order as the previous one and therefore, again contributing to the total background at the percent level. It was evaluated using a mis-tagging probability for  $c$ -jet equal to 10%.
- $qg \rightarrow q\mu^+\mu^-\nu\bar{\nu}$  ( $K = 1.3$ ): also, this background is of the same order as the previous one, contributing to the total background at the percent level. It was evaluated using mis-tagging probability for light  $q$ -jet equal to 1%.

Fig. 3 presents  $pp \rightarrow \phi^0 b \rightarrow \mu^+\mu^-b + X$  signal rates versus  $m_A$ , where  $\phi^0 = A, H, h$  after application of kinematical cuts and efficiency of  $b$ -tagging for  $\tan\beta = 5$  (black lines) and  $\tan\beta = 55$  (red lines). Results for low and high luminosity regimes are denoted by solid and dashed lines respectively.

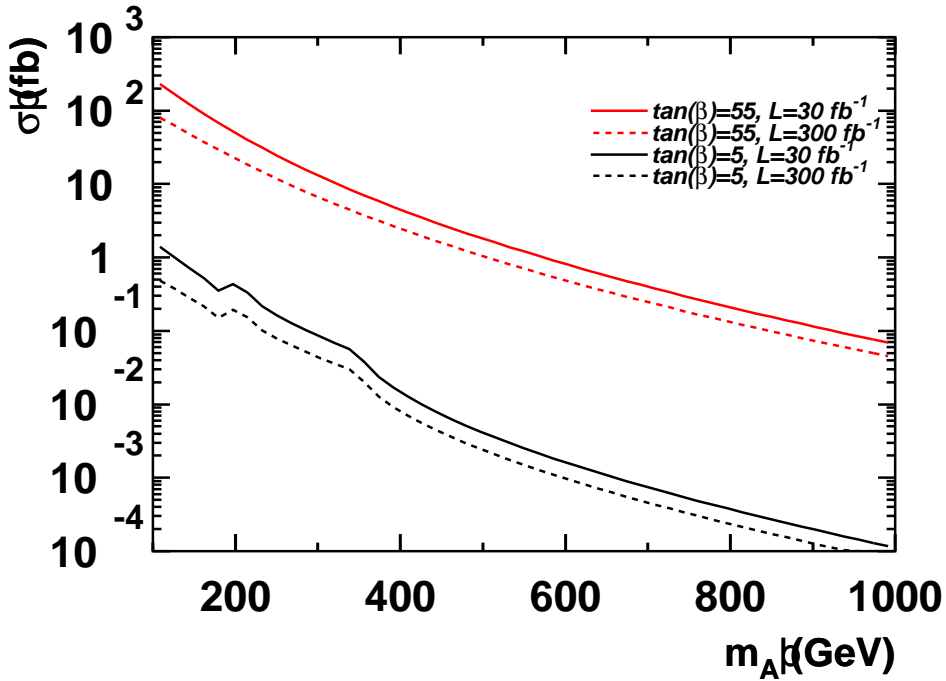


Figure 3:  $pp \rightarrow \phi b \rightarrow \mu^+\mu^-b + X$  signal rates versus  $m_A$ , where  $\phi = A, H, h$  after application of kinematical cuts and efficiency of  $b$ -tagging for  $\tan\beta = 5$  (black lines) and  $\tan\beta = 55$  (red lines). Results for low and high luminosity regimes are denoted by solid and dashed lines respectively.

In Fig. 4, we present rates for various backgrounds described above for  $\mu^+\mu^-b$  signature versus  $m_A$  after application of kinematical cuts and efficiency of  $b$ -tagging for an intermediate value of  $\tan\beta = 30$ . Results for low and high luminosity regimes are presented in left and right



frames respectively. One can see that indeed the contributions from the last three subdominant backgrounds discussed above are at the percent level.

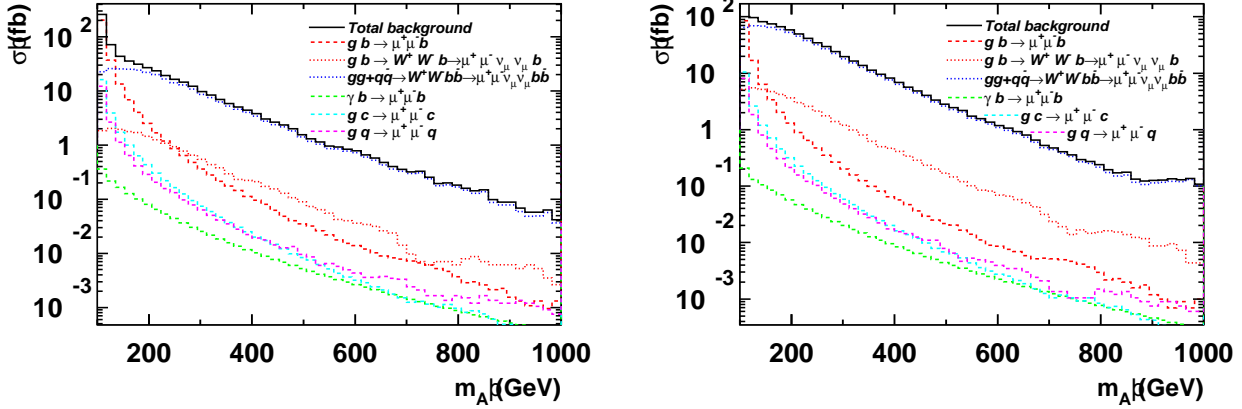


Figure 4: Rates for various backgrounds for  $\mu^+\mu^-b$  signature versus  $m_A$  after application of kinematical cuts and efficiency of  $b$ -tagging for  $\tan\beta = 30$ . Results for low and high luminosity regimes are presented in left and right frames respectively.

Using signal and background rates from these calculations, we derive the LHC discovery reach. The results are shown in Fig. 5. One should notice an important effect of the cuts for low and high luminosity regimes. The main effect for LHC reach comes from the  $MET$  cut. We require  $MET < 20$  for low luminosity which should leave signal intact assuming that instrumental missing transverse momentum is under control above 20 GeV in the low luminosity regime. This cut significantly suppresses the leading  $t\bar{t}$  background. For high luminosity regime we apply  $MET < 40$  which does not affect signal but significantly increase background. The overall effect of high luminosity cuts is an increase of the background and decrease of the signal. Therefore, the discovery potential of the LHC at  $L = 100 \text{ fb}^{-1}$  is slightly lower than at  $L = 30 \text{ fb}^{-1}$ . But in the region sufficiently above the border-line for LHC discovery potential shown in Fig. 5, say for  $m_A = 400 \text{ GeV}$  and  $\tan\beta = 55$ , LHC at  $L = 100 \text{ fb}^{-1}$  provides better statistics and significance as compared to the  $L = 30 \text{ fb}^{-1}$  case as we show below.

Here, we see that for  $L = 100 \text{ fb}^{-1}$ , the reach for  $b\phi \rightarrow b\mu^+\mu^-$  at  $\tan\beta \sim 55$  extends to  $m_A \simeq 550 \text{ GeV}$ . For  $L = 300 \text{ fb}^{-1}$ , the reach extends to  $m_A \simeq 730 \text{ GeV}$ , and for  $L = 1000 \text{ fb}^{-1}$ , the reach extends to  $\sim 925 \text{ GeV}$ .

From the results of Fig. 5, we can now compare against Fig. 2 to see how much of the  $A$ -funnel can be explored via the  $A, H \rightarrow \mu^+\mu^-$  decay mode. To illustrate, we show contours of  $m_A = 500, 750, 1000$  and  $1250$  in Fig. 2. Thus, for  $100 \text{ fb}^{-1}$  of integrated luminosity, we expect LHC to be sensitive to a  $A, H \rightarrow \mu^+\mu^-$  bump for about half of the  $A$ -funnel. An integrated luminosity of  $300 \text{ fb}^{-1}$  covers about three-quarters of the  $A$ -funnel, while well over  $1000 \text{ fb}^{-1}$  will be needed to cover the entire funnel region.

In addition to measuring the value of  $m_{A,H}$  via a dimuon mass bump, one may be able to extract information on the  $A, H$  widths from the dimuon channel, if LHC experiments have



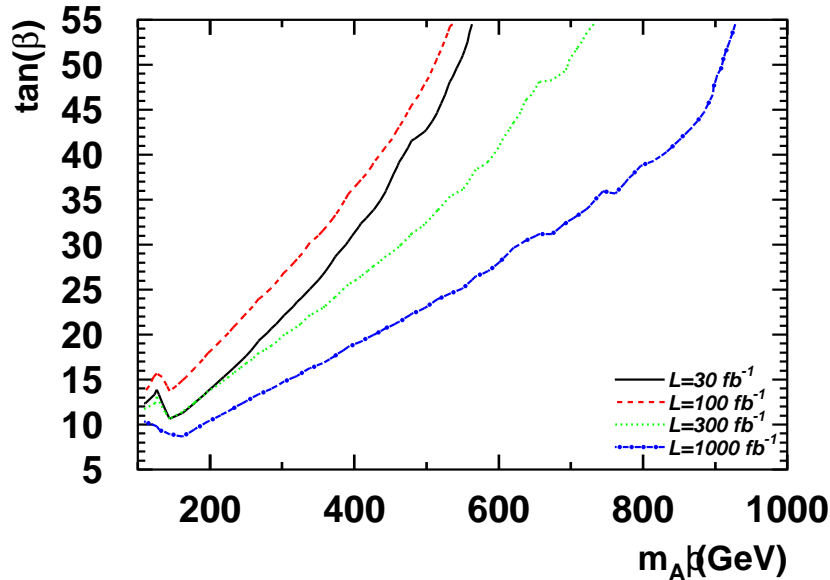


Figure 5: *LHC reach for the pseudoscalar Higgs  $A$  via  $pp \rightarrow bA \rightarrow b\mu^+\mu^- + X$  in the  $m_A$  vs.  $\tan\beta$  plane for various possible values of integrated luminosity. The  $30\text{ fb}^{-1}$  reach exceeds the  $100\text{ fb}^{-1}$  reach because we use harder cuts in the high luminosity case.*

sufficiently good muon energy reconstruction. To illustrate the values of  $\Gamma_A$  that are expected, we plot contours of  $\Gamma_A/m_A$  in Fig. 2. These range from about 5% for low  $m_{1/2} \sim 250$  GeV, corresponding to  $\Gamma_A \sim 15 - 20$  GeV, to about 4.4% for  $m_{1/2} \sim 1200$  GeV, where  $\Gamma_A \sim 50$  GeV. To better illustrate the range of Higgs widths expected in mSUGRA, we show in Fig. 6 the value of  $\Gamma_A$  versus  $m_A$  after a scan over mSUGRA parameter space for various fixed values of  $\tan\beta$ . Here, we see that indeed as  $\tan\beta$  grows, so too does  $\Gamma_A$ . In fact, for a measured value of  $m_A$ , a measurement of  $\Gamma_A$  will indicate a rather small window of allowed  $\tan\beta$  values. Naively, one might expect a one-to-one correspondence between  $\tan\beta$  and  $\Gamma_A$  for fixed  $m_A$ . However, two effects that spread out the correlation include: (i). weak scale threshold corrections to  $f_b$  that are large at large  $\tan\beta$ , and depend on the entire SUSY spectrum via loop effects [25], and (ii). various additional SUSY decay modes of the  $A$  and  $H$  may open up [26], depending on sparticle masses and mixings. For instance, if  $m_A > 2m_{\tilde{W}_1}$ , then the decay mode  $A \rightarrow \tilde{W}_1^+ \tilde{W}_1^-$  opens up and contributes to the  $A$  width. Thus, models with lighter SUSY particles should correspond to larger  $\Gamma_A$  values for a given  $m_A$  and  $\tan\beta$  value, whereas if all non-standard decay modes are closed, then the lower range of  $\Gamma_A$  that is shown may be expected to occur. The loop corrections to  $f_b$  tend to enhance  $f_b$  for  $\mu > 0$  and diminish  $f_b$  for  $\mu < 0$ , leading to somewhat separated bands for each  $\tan\beta$  value.

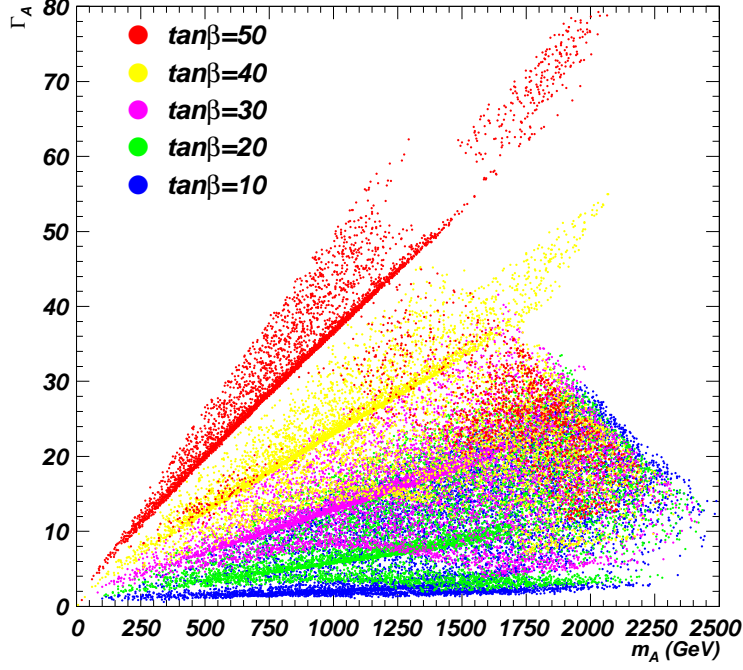


Figure 6: Plot of  $\Gamma_A$  vs.  $m_A$  from a scan over  $mSUGRA$  model parameters for  $\tan\beta = 10, 20, 30, 40$  and  $50$ .

### 3 Detailed simulations for $pp \rightarrow bA, bH + X$

In this section, we present a detailed Monte Carlo study of detection of  $b\phi \rightarrow b\mu^+\mu^-$  for a particular case study. The benchmark point we adopt is known as LCC4 in the study by Battaglia *et al.*, Ref. [27]. Some of the  $mSUGRA$  parameters and sparticle masses as generated by Isajet 7.80 are given in Table 1. We use a value of  $m_t = 175$  GeV instead of 178 GeV as in Ref. [27] since the latest Isasugra/IsaReD code gives a relic density of  $\Omega_{\tilde{Z}_1} h^2 = 0.1$  for the 175 GeV value, and 0.16 for the 178 GeV value. We also examine later how well the value of  $\Gamma_A$  can be measured for benchmark point BM600 with  $m_A = 608$  GeV.

The resolution of the dimuon invariant mass, and hence an accurate measurement of  $m_A$  and especially  $\Gamma_A$ , depends on the LHC detector's ability to measure the muon's momentum. The muon momentum is measured from its amount of bending in the magnetic field of the detector. Thus, for low energy muon, with a highly curved track, the muon  $\vec{p}$  measurement should be more precise than for high energy muons, which have very little track curvature. For our studies, we use a CMS muon smearing subroutine, where the smearing as a function of  $|\eta(\mu)|$  is displayed in Fig. 7, for several muon  $p_T$  values [28, 29].

We begin our MC simulation by calculating  $bg \rightarrow b\mu^+\mu^-$  production for  $pp$  collisions at

parameter	LCC4	BM600
$m_0$	380	900
$m_{1/2}$	420	650
$A_0$	0	0
$\tan \beta$	53	55
$\mu$	528.2	750.7
$m_{\tilde{g}}$	991.5	1502.6
$m_{\tilde{u}_L}$	973.0	1609.0
$m_{\tilde{t}_1}$	713.4	1167.9
$m_{\tilde{b}_1}$	798.9	1309.5
$m_{\tilde{e}_L}$	475.4	998.2
$m_{\tilde{e}_R}$	412.5	931.5
$m_{\tilde{\tau}_1}$	206.6	541.7
$m_{\tilde{W}_1}$	325.7	520.1
$m_{\tilde{Z}_2}$	325.4	519.5
$m_{\tilde{Z}_1}$	172.5	274.7
$m_A$	420.7	607.9
$m_H$	423.5	612.0
$m_h$	115.1	117.1
$\Delta a_\mu$	$35 \times 10^{-10}$	$11 \times 10^{-10}$
$BF(b \rightarrow s\gamma)$	$1.9 \times 10^{-4}$	$2.8 \times 10^{-4}$
$BF(B_s \rightarrow \mu^+\mu^-)$	$2.8 \times 10^{-8}$	$1.1 \times 10^{-8}$
$\Omega h_{\tilde{Z}_1}^2$	0.096	0.089
$\sigma(\tilde{Z}_1 p)$ pb	$1.1 \times 10^{-8}$	$1.7 \times 10^9$
$\Gamma_A$	19.1 GeV	31.9 GeV
$\Gamma_H$	19.2 GeV	32.1 GeV

Table 1: Masses and parameters in GeV units for Benchmark points LCC4 (with  $m_t = 175$  GeV) and BM600 (with  $m_t = 173.3$  GeV) using Isajet 7.80.

$\sqrt{s} = 14$  TeV using CalcHEP [30]. The relevant Feynman diagrams are displayed in Fig. 8. They include not only  $A$  and  $H$  production and decay, but also background contributions from  $\gamma^*$ ,  $Z^*$  and  $h$  production.

In Fig. 9, we plot the invariant mass distribution of muon pairs  $m_{\mu^+\mu^-}$  for  $L = 30 \text{ fb}^{-1}$ . For all distributions now and hereafter, we take into account detector effects of muon momenta resolution according to Fig. 7 using Gaussian smearing applied to the particle's momentum generated by CalcHEP at the parton level. What is clear from the plot is that the  $\gamma$ ,  $Z \rightarrow \mu^+\mu^-$  peaks stand out; but also the  $A$ ,  $H \rightarrow \mu^+\mu^-$  overlapping peak stands out well above background levels at  $m_A \sim 420$  GeV.

In Fig. 10, we plot the muon  $p_T$  distribution (solid line) and b-jet  $p_T$  distribution (dashed line) from  $pp \rightarrow bA \rightarrow b\mu^+\mu^- + X$  production for the LCC4 benchmark. The muon  $p_T$  distribution peaks at around  $p_T \sim m_A/2$ , but with substantial smearing to either side due to the momentum of the  $A$ . Since the  $b$ -jets are emitted preferentially in the forward direction, the

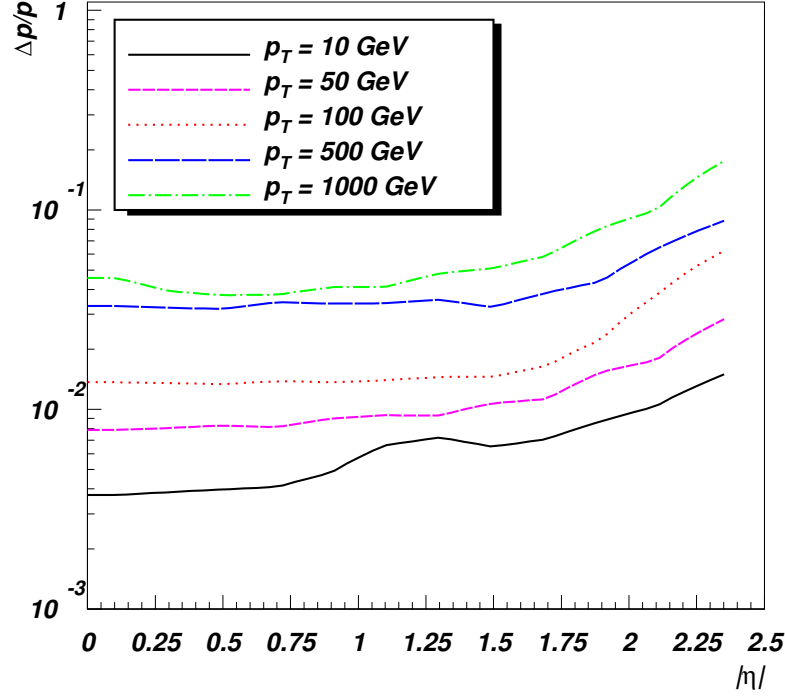


Figure 7: Plot of CMS muon smearing function versus  $|\eta(\mu)|$  for various muon  $P_T$  values.

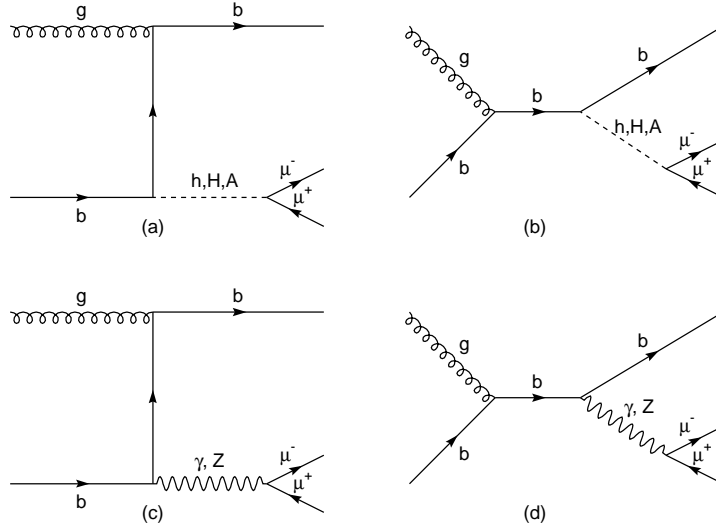


Figure 8: Feynman diagrams for  $bg \rightarrow b\mu^+\mu^-$  in the MSSM.

$p_T(b)$  distribution peaks at low values, with some smearing out to values over a hundred GeV. In Fig. 11, we plot the muon (solid line) and  $b$ -jet (dashed line) pseudo-rapidity distributions from  $pp \rightarrow bA \rightarrow b\mu^+\mu^- + X$  for the LCC4 benchmark. The muon  $\eta$  distribution is clearly more central, while  $\eta(b)$  is less central due to its role as an element in QCD initial state radiation.

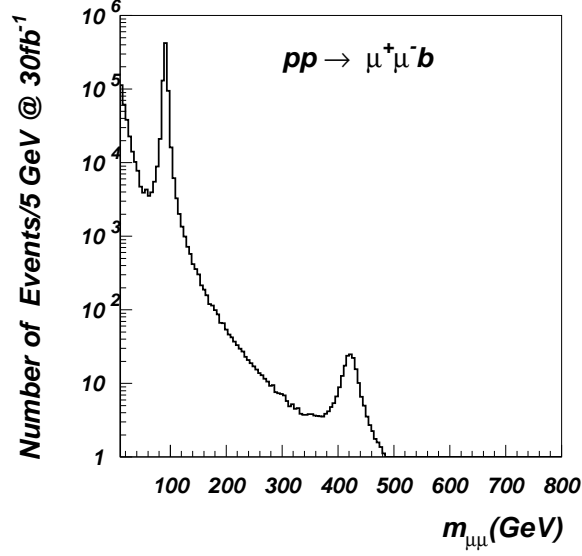


Figure 9: Plot of invariant mass distribution of muon pairs  $m_{\mu^+\mu^-}$  from a CalcHEP MC computation using benchmark LCC4.

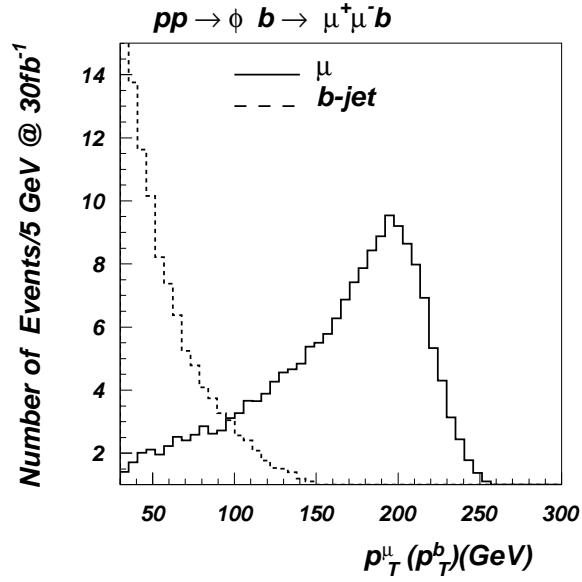


Figure 10: Plot of distribution in  $p_T(\mu)$  (solid line) and  $p_T(b)$  (dashed line) from a CalcHEP MC computation using benchmark LCC4.

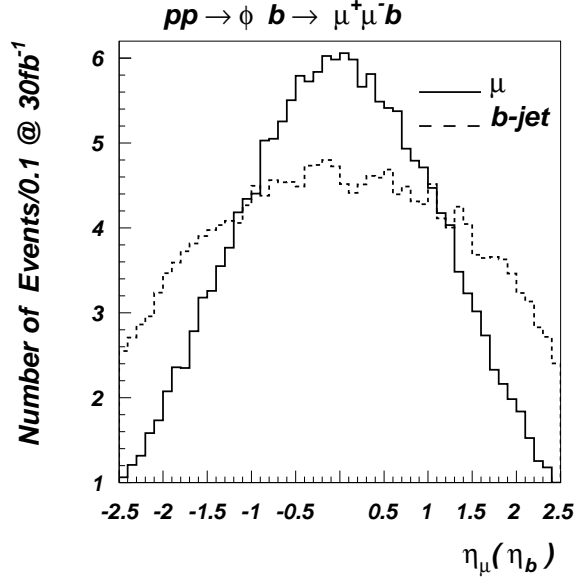


Figure 11: Plot of distribution in  $\eta(\mu)$  (solid line) and  $\eta(b)$  (dashed line) from a CalcHEP MC computation using benchmark LCC4.

## 4 Extracting $m_{A,H}$ and $\Gamma_{A,H}$

Once a dimuon mass bump has been established, the next step is to fit the invariant mass distribution with a curve which depends on the Higgs mass and width. A complication occurs because in our case the  $A$  and  $H$  masses are only separated by  $\sim 3$  GeV, and so the two peaks are highly overlapping, and essentially indistinguishable. To see what this means for an ideal measurement, we plot in Fig. 12 for LCC4 the dimuon invariant mass from just the reaction  $pp \rightarrow bA \rightarrow b\mu^+\mu^- + X$  (red curve), and also the distribution from  $pp \rightarrow bH \rightarrow b\mu^+\mu^- + X$  (blue curve), along with the sum (black curve). A direct measurement of these idealized distributions of full-width-at-half-max shows indeed that  $\Gamma_A \simeq 430 - 410 = 20$  GeV, while  $\Gamma_H \simeq 433 - 413 = 20$  GeV. A measure of the summed distributions provides  $\Gamma_{A,H} \simeq 433 - 410 = 23$  GeV, *i.e.* the idealized width expectation expanded by the  $A$ ,  $H$  mass splitting. We fit the dimuon invariant mass distribution from all diagrams of Fig. 8 along with muon smearing with the following function  $F$  of dimuon mass  $m$  and 6 fitting parameters  $\Gamma, M, N, \sigma, N_{p1}, N_{p2}$ :

$$F(m; \Gamma, M, N, \sigma, N_{p1}, N_{p2}) = N \int B(m', \Gamma, M) \times G(m', m, \sigma) dm' + N_{p1} \exp(-N_{p2}m), \quad (5)$$

where  $N$  is just a normalization parameter,

$$B(m', \Gamma, M) = \frac{2}{\pi} \frac{\Gamma^2 M^2}{(m'^2 - M^2)^2 + m'^4 (\Gamma^2 / M^2)},$$

$$G(m', m, \sigma) = \frac{1}{\sqrt{2\pi}\sigma} \exp \left[ -\frac{(m' - m)^2}{2\sigma^2} \right].$$

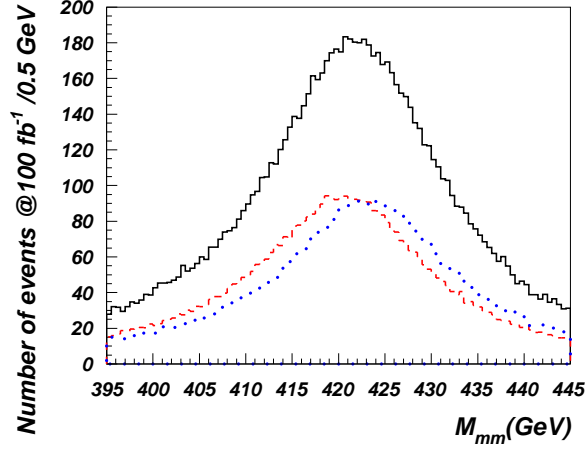


Figure 12: Plot of dimuon invariant mass ( $M_{\mu^+\mu^-}$ ) from  $bA$  production (red),  $bH$  production (blue) and sum (black) for benchmark LCC4 with no smearing.

One can see that  $F(m; \Gamma, M, N, \sigma, N_{p1}, N_{p2})$  is a convolution of the Breit-Wigner resonance function along with Gaussian detector smearing plus an exponentially dropping function describing the background shape.

The results from the  $\chi^2$  fits of signal-plus-background are presented in Fig. 13 for different integrated luminosities of  $L = 30, 100, 300$  and  $1000 \text{ fb}^{-1}$ . The left side of the Fig. 13 shows the fit to Monte Carlo data for LCC4 with  $pp \rightarrow bA, H \rightarrow b\mu^+\mu^- + X$  production including muon smearing. It also shows the values of the fitted parameters ( $\Gamma, M, N, \sigma, N_{p1}, N_{p2}$ ) together with their standard deviations according to the fit. The fit has been performed using the MINUIT program from CERN library which properly takes into account the correlation matrix of the fit parameters, which is crucial for the evaluation of the corresponding contours in the  $\Gamma_A$  vs.  $m_A$  plane at  $1\sigma$  and  $2\sigma$  confidence levels; these are shown on the right side of the Fig. 13. The black crosses show the width measurement assuming the Higgs masses are known to perfect accuracy. From Fig. 13, one can see that for  $L = 30 \text{ fb}^{-1}$  of data, the statistics only provide a rough fit to the  $A, H$  width. On the other hand, moving to  $L = 100 \text{ fb}^{-1}$ , our fit provides promising results for  $\Gamma_A$ . We see that with  $L = 100 \text{ fb}^{-1}$ ,  $m_A$  can be measured to 1 GeV accuracy, or 0.25%. Meanwhile, the  $A, H$  width is measured at  $\Gamma_{A,H} \simeq 20 \pm 8 \text{ GeV}$ , or 40% level. At higher integrated luminosity values of  $L = 300 \text{ fb}^{-1}$ , the accuracy on  $m_{A,H}$  is improved to sub-GeV levels and  $\Gamma_{A,H}$  is found to be  $\sim 20 \pm 4 \text{ GeV}$ , a 20% measurement. At  $L = 1000 \text{ fb}^{-1}$ , which might be reached in  $\sim 10$  years of LHC running, the measurement of  $\Gamma_{A,H}$  can be improved to about  $20 \pm 1.75 \text{ GeV}$ , or  $\sim 8\%$  accuracy. The  $\Gamma_{A,H}$  accuracy is expected to approach  $\sim 7\%$  level for infinite integrated luminosity, and is mainly limited by the detector muon energy resolution of 4%, which is actually quite close to  $\Gamma_A/m_A$ .

The results from the  $\chi^2$  fits to  $m_A$  and  $\Gamma_A$  of signal-plus-background for benchmark point BM600 are shown in Fig. 14 for integrated luminosities of  $L = 300$  and  $1000 \text{ fb}^{-1}$ . In this case, the heavy Higgs masses are  $m_{A,H} = 608, 612 \text{ GeV}$ , while the widths from CalcHEP are  $\Gamma_{A,H} = 31.9 (32.1) \text{ GeV}$ . We find for  $10^3 \text{ fb}^{-1}$  of integrated luminosity, that  $\Gamma_A$  is extracted to



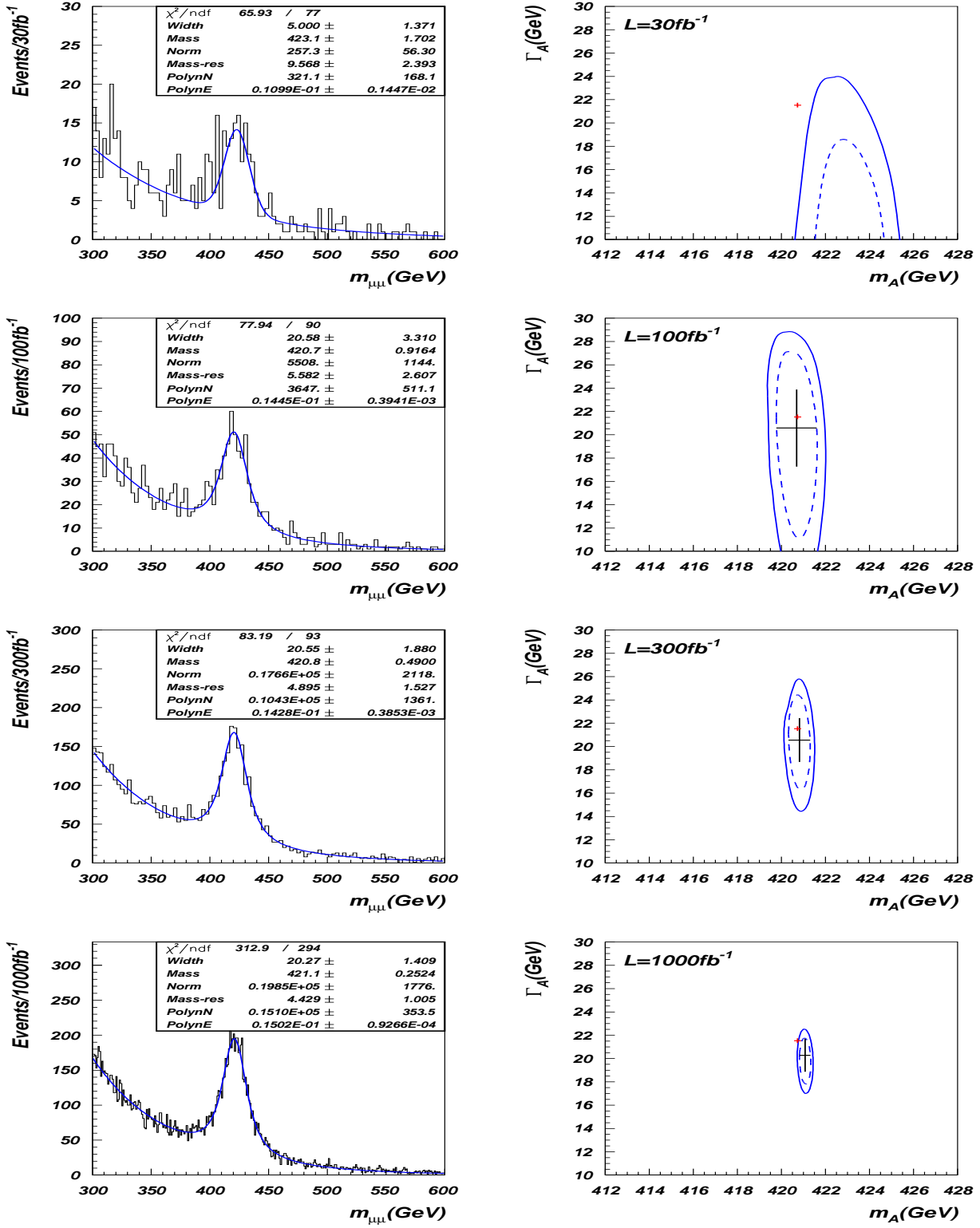


Figure 13: Left : best fit of Monte Carlo data for LCC4 for  $pp \rightarrow bA, H \rightarrow b\mu^+\mu^- + X$  production including muon smearing. Right: corresponding contours of fit to  $m_A$  and  $\Gamma_A$  values for Monte Carlo data for LCC4 from  $pp \rightarrow bA, H \rightarrow b\mu^+\mu^- + X$  production including muon smearing.

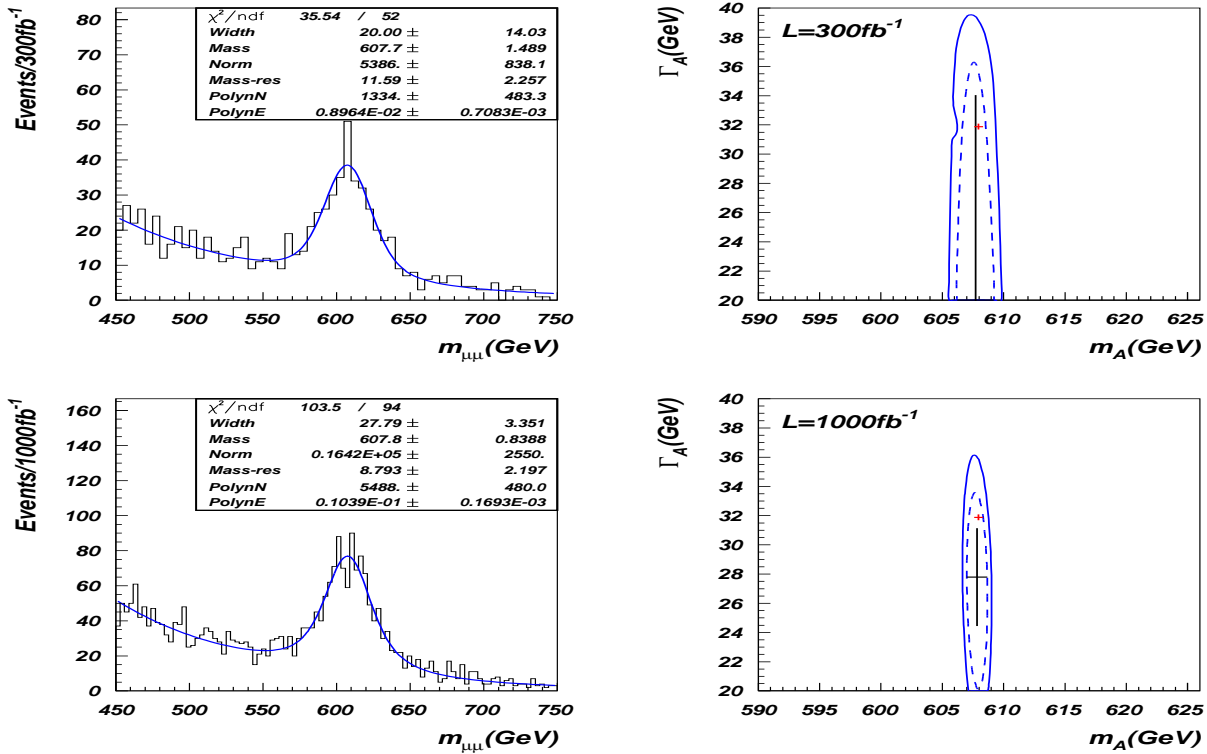


Figure 14: Left : best fit of Monte Carlo data for BM600 for  $pp \rightarrow bA, H \rightarrow b\mu^+\mu^- + X$  production including muon smearing. Right: corresponding contours of fit to  $m_A$  and  $\Gamma_A$  values for Monte Carlo data for BM600 from  $pp \rightarrow bA, H \rightarrow b\mu^+\mu^- + X$  production including muon smearing.

be  $\Gamma_A = 28 \pm 5.5 \text{ GeV}$ , a 17% measurement.

## 5 Conclusions

In  $R$ -parity-conserving supersymmetric models where the lightest neutralino is expected to be a thermal relic of the Big Bang, and to comprise the dark matter in the universe, special qualities are needed to enhance the dark matter annihilation rates. One compelling case is neutralino annihilation through the pseudoscalar Higgs resonance. Can the LHC tell us if such a mechanism is operative in the early universe? The crucial test here is whether the condition  $2m_{\tilde{Z}_1} \sim m_A$  is fulfilled.

A variety of techniques have been proposed for extracting the SUSY particle masses — including  $m_{\tilde{Z}_1}$  — in sparticle cascade decay events at the LHC [31]. Extracting the heavy Higgs masses is also possible provided that  $m_A$  is small enough and that  $\tan\beta$  is large enough. Mass measurements of heavy Higgs decays into  $b\bar{b}$  and  $\tau^+\tau^-$  are fraught with uncertainties from multi-particle production and energy loss from neutrinos. We focused instead on the suppressed decay  $A, H \rightarrow \mu^+\mu^-$ , since it allows for both highly accurate heavy Higgs mass and width reconstructions. Production of  $A$  and  $H$  in association with a single  $b$ -jet offers a

large background rejection at small cost to signal, especially in the large  $\tan\beta$  regime, where Higgs production in association with  $bs$  is expected to be enhanced by large Yukawa couplings. This is also the regime in models such as mSUGRA where neutralino annihilation through the heavy Higgs resonance is expected to occur.

In this paper, we have computed regions of  $m_A$  vs.  $\tan\beta$  parameter space where  $pp \rightarrow b\phi + X, \phi = H, A$  production followed by  $H, A \rightarrow \mu^+\mu^-$  should be visible for various integrated luminosities. We have also performed detailed Monte Carlo simulations of signal and background for the LCC4 and BM600 benchmark points. Fits of the dimuon mass spectra allow for sub-percent determinations of the (nearly overlapping)  $H$  and  $A$  masses. The  $A, H$  overlapping widths were determined to  $\sim 8\%$  ( $\sim 17\%$ ) accuracy in the case of LCC4 (BM600) with  $10^3 \text{ fb}^{-1}$  of integrated luminosity. We conclude that indeed the study of  $pp \rightarrow b\phi + X, \phi = H, A$  production followed by  $H, A \rightarrow \mu^+\mu^-$  offers a unique opportunity to directly measure  $A(H)$  Higgs width. This process also allows to measure the  $A$  ( $H$ ) mass with unprecedented precision. Both these measurements would provide crucial information to connect the cosmological  $A$  – *funnel* scenario of dark matter annihilation with LHC data. Combining these measurements with SUSY particle mass measurements such as the mass edge in  $m_{\ell^+\ell^-}$  from  $\tilde{Z}_2 \rightarrow \tilde{Z}_1 \ell^+ \ell^-$  decay would go a long way towards determining the parameter  $\tan\beta$ , and also whether or not neutralino annihilation through the  $A$  resonance (with  $2m_{\tilde{Z}_1} \sim m_A$ ) is the operative mechanism in the early universe to yield the measured abundance of neutralino dark matter.

## Acknowledgements

This research was supported in part by the U.S. Department of Energy under Grant No. DE-FG02-04ER41305 and Royal Society Grant No. 508786101. PS thanks NExT Institute as a part of SEPnet for support.

## References

- [1] For reviews, see *e.g.* C. Jungman, M. Kamionkowski and K. Griest, *Phys. Rept.* **267** (1996) 195; A. Lahanas, N. Mavromatos and D. Nanopoulos, *Int. J. Mod. Phys. D* **12** (2003) 1529; M. Drees, hep-ph/0410113; K. Olive, “Tasi Lectures on Astroparticle Physics”, astro-ph/0503065; G. Bertone, D. Hooper and J. Silk, *Phys. Rept.* **405** (2005) 279.
- [2] H. Baer and A. Box, *Eur. Phys. J. C* **68** (2010) 523; H. Baer, A. Box and H. Summy, *J. High Energy Phys.* **1010** (2010) 023.
- [3] E. Komatsu *et al.* (WMAP collaboration), arXiv:1001.4538 (2010).
- [4] A. G. Riess *et al.*, *Astrophys. J.* **699** (2009) 539 and arXiv:1103.2976 (2011).
- [5] J. Ellis, T. Falk and K. Olive, *Phys. Lett. B* **444** (1998) 367; J. Ellis, T. Falk, K. Olive and M. Srednicki, *Astropart. Phys.* **13** (2000) 181; M.E. Gómez, G. Lazarides and C. Pallis, *Phys. Rev. D* **61** (2000) 123512 and *Phys. Lett. B* **487** (2000) 313; A. Lahanas, D. V. Nanopoulos and V. Spanos, *Phys. Rev. D* **62** (2000) 023515; R. Arnowitt, B. Dutta and Y. Santoso, *Nucl. Phys. B* **606** (2001) 59; see also Ref. [17].

- [6] C. Böhm, A. Djouadi and M. Drees, *Phys. Rev.* **D 30** (2000) 035012; J. R. Ellis, K. A. Olive and Y. Santoso, *Astropart. Phys.* **18** (2003) 395; J. Edsjö, *et al.*, JCAP **0304** (2003) 001
- [7] K. Griest and D. Seckel, *Phys. Rev.* **D 43** (1991) 3191; J. Edsjo and P. Gondolo, *Phys. Rev.* **D 56** (1997) 1879; J. Edsjo, M. Schelke, P. Ullio and P. Gondolo, JCAP **0304** (2003) 001 [arXiv:hep-ph/0301106].
- [8] N. Arkani-Hamed, A. Delgado and G. Giudice, *Nucl. Phys.* **B 741** (2006) 108; H. Baer, A. Mustafayev, E. Park and X. Tata, JCAP**0701**, 017 (2007) and *J. High Energy Phys.* **0805** (2008) 058.
- [9] K. L. Chan, U. Chattopadhyay and P. Nath, *Phys. Rev.* **D 58** (1998) 096004; J. Feng, K. Matchev and T. Moroi, *Phys. Rev. Lett.* **84** (2000) 2322 and *Phys. Rev.* **D 61** (2000) 075005; see also H. Baer, C. H. Chen, F. Paige and X. Tata, *Phys. Rev.* **D 52** (1995) 2746 and *Phys. Rev.* **D 53** (1996) 6241; H. Baer, C. H. Chen, M. Drees, F. Paige and X. Tata, *Phys. Rev.* **D 59** (1999) 055014; for a model-independent approach, see H. Baer, T. Krupovnickas, S. Profumo and P. Ullio, *J. High Energy Phys.* **0510** (2005) 020.
- [10] M. Drees and M. Nojiri, *Phys. Rev.* **D 47** (1993) 376; H. Baer and M. Brhlik, *Phys. Rev.* **D 57** (1998) 567; H. Baer, M. Brhlik, M. Diaz, J. Ferrandis, P. Mercadante, P. Quintana and X. Tata, *Phys. Rev.* **D 63** (2001) 015007; J. Ellis, T. Falk, G. Ganis, K. Olive and M. Srednicki, *Phys. Lett.* **B 510** (2001) 236; V. D. Barger and C. Kao, *Phys. Lett. B* **518** (2001) 117; L. Roszkowski, R. Ruiz de Austri and T. Nihei, *J. High Energy Phys.* **0108** (2001) 024; A. Djouadi, M. Drees and J. L. Kneur, *J. High Energy Phys.* **0108** (2001) 055; A. Lahanas and V. Spanos, *Eur. Phys. J. C* **23** (2002) 185.
- [11] H. Baer, A. Mustafayev, S. Profumo, A. Belyaev and X. Tata, *Phys. Rev.* **D 71** (2005) 095008; H. Baer, A. Mustafayev, S. Profumo, A. Belyaev and X. Tata, *J. High Energy Phys.* **0507** (2005) 065.
- [12] H. Baer, C. H. Chen, M. Drees, F. Paige and X. Tata, *Phys. Rev. Lett.* **79** (1997) 986.
- [13] J. Campbell, R. K. Ellis, F. Maltoni and S. Willenbrock, *Phys. Rev.* **D 67** (2003) 095002.
- [14] C. Kao, D. A. Dicus, R. Malhotra and Y. Wang, *Phys. Rev. D* **77** (2008) 095002; C. Kao, S. Sachithanandam, J. Sayre and Y. Wang, *Phys. Lett. B* **682** (2009) 291.
- [15] C. Kao, N. Stepanov, *Phys. Rev.* **D52**, 5025-5030 (1995).
- [16] S. Dawson, D. Dicus, C. Kao and R. Malhotra, *Phys. Rev. Lett.* **92** (2004) 241801; C. Kao and Y. Wang, *Phys. Lett. B* **635** (2006) 30.
- [17] IsaReD, by H. Baer, C. Balazs and A. Belyaev, *J. High Energy Phys.* **0203** (2002) 042.
- [18] ISAJET v7.79, by H. Baer, F. Paige, S. Protopopescu and X. Tata, hep-ph/0312045; for details on the Isajet spectrum calculation, see H. Baer, J. Ferrandis, S. Kraml and W. Porod, *Phys. Rev.* **D 73** (2006) 015010.
- [19] H. Baer, C. Balazs, A. Belyaev, T. Krupovnickas and X. Tata, *J. High Energy Phys.* **0306** (2003) 054

- [20] H. Baer, J. Ellis, G. Gelmini, D. V. Nanopoulos and X. Tata, *Phys. Lett. B* **161** (1985) 175; G. Gamberini, *Z. Physik C* **30** (1986) 605; H. Baer, V. Barger, D. Karatas and X. Tata, *Phys. Rev. D* **36** (1987) 96; H. Baer, X. Tata and J. Woodside, *Phys. Rev. D* **45** (1992) 142.
- [21] H. Baer and J. O’Farrill, JCAP**0404**, 005 (2004); H. Baer, A. Belyaev, T. Krupovnickas and J. O’Farrill, JCAP **0408** (2004) 005; H. Baer, E. K. Park and X. Tata, *New J. Phys.* **11** (2009) 105024.
- [22] E. Aprile *et al* (Xenon100 Collaboration), *Phys. Rev. Lett.* **105** (2010) 131302.
- [23] H. Baer, K. Hagiwara and X. Tata, *Phys. Rev. D* **35** (1987) 1598; H. Baer, D. Dzialo-Karatas and X. Tata, *Phys. Rev. D* **42** (1990) 2259; H. Baer, C. Kao and X. Tata, *Phys. Rev. D* **48** (1993) 5175; H. Baer, C. H. Chen, F. Paige and X. Tata, *Phys. Rev. D* **50** (1994) 4508; I. Hinchliffe *et al.*, *Phys. Rev. D* **55** (1997) 5520 and *Phys. Rev. D* **60** (1999) 095002; H. Bachacou, I. Hinchliffe and F. Paige, *Phys. Rev. D* **62** (2000) 015009.
- [24] S. Kretzer, H. L. Lai, F. I. Olness and W. K. Tung, *Phys. Rev. D* **69**, 114005 (2004) [arXiv:hep-ph/0307022].
- [25] D. Pierce, J. Bagger, K. Matchev and R. Zhang, *Nucl. Phys. B* **491** (1997) 3.
- [26] H. Baer, M. Bisset, D. Dicus, C. Kao and X. Tata, *Phys. Rev. D* **47** (1993) 1062; H. Baer, M. Bisset, C. Kao and X. Tata, *Phys. Rev. D* **50** (1994) 316.
- [27] E. Baltz, M. Battaglia, M. Peskin and T. Wizansky, *Phys. Rev. D* **74** (2006) 103521.
- [28] G. L. Bayatian *et al.* [CMS Collaboration],
- [29] G. L. Bayatian *et al.* [CMS Collaboration], *J. Phys. G* **34**, 995 (2007).
- [30] CalcHEP, by A. Pukhov, hep-ph/0412191.
- [31] For a review, see *e.g.* A. J. Barr and C. G. Lester, *J. Phys. G* **37** (2010) 123001.